J Mol Model (2011) 17:3129–3149
DOI 10.1007/s00894-011-0998-3

ORIGINAL PAPER

Molecular dynamics simulation of the *Staphylococcus aureus* YsxC protein: molecular insights into ribosome assembly and allosteric inhibition of the protein

Amit Goyal · Kannan Muthu · Manivel Panneerselvam · Anil Kumar Pole · Krishna Ramadas

Received: 4 October 2010 / Accepted: 26 January 2011 / Published online: 2 March 2011

Abstract YsxC from *Staphylococcus aureus* is a member of the GTPase protein family, and is involved in the ribosomal assembly and stability of this microorganism through its interactions with the L17, S2 and S10 ribosomal proteins. Inhibition of its interactions with L17, S2, S10 and the β′ subunit of RNA polymerase influences ribosomal assembly, which may affect the growth of the microorganism. This makes YsxC a novel target for the design of inhibitors to treat the disease caused by *S. aureus*. Understanding the interaction mechanism between YsxC and its partners would aid in the identification of potential catalytic residues, which could then be targeted to inhibit its function. Accordingly, in the present study, an in silico analysis of the interactions between YsxC and L17, S2 and S10 was performed, and the potential residues involved in these interactions were identified. Based on the simulation results, a possible mechanism for the interactions between these proteins was also proposed. Finally, six ligands from among a library of 81,000 chemical molecules were found to interact with parts of the G2 and switch II regions of the YsxC protein. Moreover, their interactions with the YsxC protein were observed to provoke changes at its GTP-binding site, which suggests that the binding of these ligands leads to a reduction in GTPase activity, and they were also found to affect the interactions of YsxC with its partners. This observation indicates that the proposed interacting site of YsxC may act as an allosteric site, and disrupting interactions at this site might lead to novel allosteric inhibition of the YsxC protein.

Keywords YsxC · *Staphylococcus aureus* · Homology modeling · Molecular dynamics simulation · Molecular docking · Protein–protein interaction

Introduction

Staphylococcus aureus is a notorious bacterium that has the ability to evolve into new virulent types and drug-resistant variants [1]. Nosocomial infections of *S. aureus* have produced serious public health issues in recent years [2]. Humans are natural reservoirs for *S. aureus*, and it colonizes the nares and skin of approximately 20–30% of healthy adults [3, 4]. *S. aureus* infection is of special concern because of its various serious complications, such as skin infections, bacteremia, osteomyelitis, endocarditis, septic arthritis, and toxic shock syndrome [3]. A loss of skin barrier integrity [5] (e.g., in surgical patients, kidney dialysis patients, trauma and burn patients, etc.) and decreased immunity (e.g., in immune-compromised individuals, such as cancer and AIDS patients) are the causes of this infection [6, 7]. The increasing resistance of *S. aureus* to current antibiotics such as penicillin, ampicillin, methicillin, amoxicillin, and the recently developed vancomycin [8, 9] has led to the search for novel drug targets.

Recently, genome mining has identified 15 essential proteins in the genome of *S. aureus* that belong to the low molecular weight GTPase superfamily [10]. YsxC, one of the identified low molecular weight GTPases, is an ortholog of the Era/Obg family of GTP-binding proteins, and was

Amit Goyal and Muthu Kannan contributed equally to this work.

A. Goyal · K. Muthu · M. Panneerselvam · A. K. Pole · K. Ramadas (✉)
Centre of Excellence in Bioinformatics, School of Life Sciences, Pondicherry University,
Puducherry 605 014, India
e-mail: krishstrucbio@gmail.com

found to be a significant influence on the life span of *S. aureus* [11]. In *S. aureus*, YsxC associates with the 50S subunit in a similar way to its homolog in *B. subtilis* [12–14]. Co-fractionation experiments confirm the interaction of YsxC with L17 from the 50S large subunit and S2 and S10 from the 30S small subunit of the ribosome as well as with the β′ subunit of RNA polymerase [12]. These interactions influence the stability of the ribosome assembly and in turn affect protein synthesis. Inhibiting the mechanism for the interactions of YsxC with its partners may affect the transcription machinery and influence the life span of the bacterium. The functional importance of YsxC makes it an interesting drug target for treating the infections caused by this bacterium.

Disrupting the interactions of this protein with its partners and disturbing the binding of GTP could provide a way to target this function. However, the utilization of binding sites other than those for GTP and YsxC's interaction partners could possibly result in structural transformations that affect the entire functionality of this protein. Identifying the sites that induce the allosteric inhibition mechanism has proven to be an efficient approach for many such proteins [15, 16]. However, the unavailability of structural information for YsxC and its interaction partners has initiated for structure-based drug design. An initial attempt to formulate a protocol for a structure-based drug-design approach that targets YsxC was made in this study. Primarily, the three-dimensional structures of YsxC and its interaction partners were identified, and the structure of GTP-bound YsxC was then generated. The mechanism of interactions of the GTP-bound YsxC with its partners was analyzed through in silico interaction methodologies, and the sites involved in these interactions were identified. Finally, the ligands were retrieved from ligand databases, and their abilities to introduce structural changes by binding at sites other than those for GTP and interacting partners of YsxC were analyzed. The results reveal the possibility of a site close to the GTP-binding site affecting the allosteric inhibition of YsxC, as evidenced by the structural changes induced by the binding of six different ligands at this site. The results obtained could pave a novel path towards the design of structure-based inhibitors for YsxC.

Materials and methods

Tertiary structure prediction

Homology modeling was used to generate the 3D structure of the proteins. Protein sequences for *S. aureus* YsxC (196aa, UniProtKB accession number: C8ASR9), L17 (122aa, UniProtKB accession number: C8AMP1), S2 (255aa, UniProtKB accession number: C8ARE0) and S10 (102aa, UniProtKB accession number: C8AMR9) were retrieved from UniProt (http://www.uniprot.org). A $BLAST_P$ search was carried out against the PDB database (PDB, http://www.rscb.org/pdb/) to detect the most suitable template for homology modeling. The closest structural template for YsxC (PDB ID: 1SUL [17], chain A) was apo-YsxC from *Bacillus subtilis*, with 57% sequence identity, which was therefore chosen for structural modeling. Similarly, bacteria-specific L17 (PDB ID: 1GD8 [18], chain A) from *Thermus thermophilus* (47% identity), 30S ribosomal protein S2 (PDB ID: 1FJG [19], chain B) from *Thermus thermophilus* (54% identity), and S10 (PDB ID: 1P6G [20], chain J) from *Escherichia coli* (62% identity) were selected for L17, S2, and S10 respectively. ClustalW2 [21] was used to perform the alignment of the query and template sequences. The aligned sequences were passed to Modeler9v7 for model generation [22, 23]. The best models were chosen based on the discrete optimized protein energy (DOPE) and objective function (MOF) scores and subjected to MDS using the GROMACS 4.0.7 [24] package for structural refinement.

MDS of homology models

The GROMACS 4.0.7 molecular dynamics package and OPLS-AA [25] all-atom force field were used to analyze model stability. The protein models were solvated with the Monte Carlo simulated TIP3P [26] water model using a 1-nm triclinic box. Periodic boundary conditions were applied in all directions, and the system was neutralized by replacing water molecules with sodium and chloride counterions. L17 and S10 were neutralized by the addition of six Cl^- ions, while S2 was neutralized by adding five Na^+ ions. Subsequently, a maximum of 50,000 energy minimization steps were carried out for the constructed models using a steepest descent algorithm with a tolerance of 1000 kJ mol^{-1} nm^{-1}. A twin-range cutoff was applied to long-range interactions using the PME [27] method: 1.0 nm for van der Waals and electrostatic interactions. These minimized and solvated systems were considered reasonable structures in terms of geometry and solvent orientations and used in further simulations. All bond angles were constrained with the LINCS [28] algorithm, while the geometry of the water molecules was constrained with the SATTLE [29] algorithm. The weak coupling method V-rescale was used to regulate the temperature, while the Parrinello–Rahman method [30] was used to set the pressure of the system. Equilibration MD for both temperature (300 K) and pressure (1 atm) were carried out for 100 ps. We observed that the temperature, pressure, density and total energy of the system were well equilibrated. These pre-equilibrated systems were subsequently used in the

3000 ps (3 ns) production MDS with a time-step of 2 fs. Structural coordinates were saved every 2 ps and analyzed using the analytical tools in the GROMACS package. The lowest potential energy conformations were selected from the 3 ns MDS trajectory and further refined by energy minimization. The refined models were validated using the structural analysis and verification server (SAVES), which uses various tools, including PROCHECK [31], ERRAT [32], and VERIFY_3D [33].

Binding pocket prediction of YsxC

The Protein Structure and Function Prediction Resource (PSiFR) [34] and Q-SiteFinder [35] were used to measure the volume of each pocket, in terms of both solvent-accessible surface and molecular surface, in order to find the ligand-binding and active sites of the protein. Motif Scan [36] and the NCBI Conserved Domain Search (CD search) [37, 38] were used to find the functional motifs and conserved domains in the modeled YsxC structure, respectively. Results obtained from the above predictions were used to define the GTP-binding site and the allosteric site of the YsxC protein.

Molecular docking and MDS studies of YsxC–GTP and YsxC–ligand complexes

Docking of GTP at the active site of YsxC

The lowest-energy minimized protein structure of YsxC found via MDS was selected for docking studies. The protein was prepared by a multistep process using the Protein Preparation Wizard of the Schrödinger 2009 suite (Schrödinger LLC, New York, USA). The GTP structure was drawn in SDF format using the MarvinSketch tool and prepared using the LigPrep (version 2.3; Schrödinger LLC) module for docking. The prepared protein was employed to build energy grids using the protein atom scaling parameters (1.0) within a cubic box of dimensions 31.000 Å× 48.127 Å×32.274 Å centered on the centroid of the active site residues. The bounding box dimensions (within which the centroid of a docked pose was confined) were set to be 14 Å×14 Å×14 Å. Induced Fit Docking Panel was used to observe the docking interaction of GTP with YsxC. The extra precision (XP) docking and scoring mode was chosen for Glide re-docking.

Docking of ligands at the allosteric site of YsxC

A database of around 81,000 drug-like compounds was downloaded from the Ligand.Info small-molecule meta-database [39], and further screened based on ADME/T properties and reactive functional groups by QikProp 3.2 Panel in the Schrödinger suite. Around 10,230 successfully processed and selected ligands (based on descriptors and property values) were prepared by the LigPrep module. A grid was generated by defining the allosteric site residues for YsxC using the Receptor Grid Generation panel in the Glide 5.5 module. Initially, all of the 23,354 ligands prepared via LigPrep were docked using a high-throughput virtual screening (HTVS) protocol for the rapid screening of ligands. The 3,342 ligands with a docking score above the cutoff value of −5.0 were subjected to a standard precision (SP) docking protocol. From these, 392 ligands were selected (using a cutoff Glide score of −7.5) for the XP docking protocol. After removing redundancy, the top 20 ligands were considered for further inspection. The individual interactions of the ligands with the protein residues within the binding cavity and energetically favorable interactions were the criteria for inspection. The ligands were rejected if they were present outside the binding cavity. A total of six ligands were selected for further analysis of binding interactions. The ligand that showed the most energetically favorable interactions was selected and subjected to induced-fit docking to observe the conformational changes in the protein.

Docking of GTP in the presence of the ligand

Induced-fit docking of the protein–ligand complex with GTP was performed by defining the GTP binding site for interaction in the Glide grid setup. This helped to clarify how the GTP binding is affected by the binding of a ligand at the allosteric site. The XP docking and scoring mode was chosen for Glide re-docking. Energy minimization and MDSs were carried out for the YsxC–GTP, YsxC–Ligand 3 and YsxC–GTP–Ligand 3 complexes to check the sustainability of both GTP and the ligand in their corresponding binding pockets. MDS was performed using GROMACS 4.0.7 with the previously described parameters. Ligand topologies for MDS were generated using PRODRG2 server [40]. The lowest-energy structures from 3 ns MDS were used to check the residues involved in the protein–ligand interaction and the interaction energies. Molecular graphical representations of these complexes were prepared using the PyMOL visualization software.

Protein–protein interaction site prediction

Many tools are available that can assist in the prediction of interface residues and also help in predicting the structure of the intermolecular complex formed between two or more molecules. What Information Does Surface Conservation Yield (WHISCY) [41] was used for interface predictions, and the results were passed to WHISCYMATE for consensus scoring. The refined protein files for YsxC,

L17, S2 and S10 along with the chain ID and the pairwise sequence alignment file were uploaded for WHISCYMATE prediction. The interface residues were predicted based on conservation and structural information for the template protein, and these results were used for further analysis. Similarly, Protein–Protein Interaction Site Predictor (cons-PPISP) [42, 43] consensuses were used to find the interface sites. We also used PatchDock server [44, 45] to find the interacting residues in the YsxC–L17, YsxC–S2 and YsxC–S10 complexes without specifying any binding site, and these results were refined using the FireDock [46] method. The interacting residues present in each protein–protein complex supported the interface residues predicted by the WHISCY program. The interface predictions were used to define ambiguous interaction restraints (AIRs), where predicted residues are designated as active residues and their surface neighbors as passive residues. The interface amino acid residues that constitute the flexible segments were defined by the active and passive amino acid residues used in the AIRs ± 2 sequential residues.

Protein–protein interaction studies

The structures of the protein–protein complexes (YsxC–L17, YsxC–S2 and YsxC–S10) were determined using docking software. The docking was performed using High Ambiguity Driven Biomolecular Docking (HADDOCK 2.0) [47, 48] from an ensemble of structures. For each protein, ten different conformations were drawn from the 3 ns MDS trajectory starting from 1.2 ns at intervals of 0.2 ns up to 3 ns for docking purposes. The ambiguous interaction restraints (AIRs) that were used to drive the docking process were defined using the interface predictions mentioned above.

The docking was performed based on ten conformations of each protein, in other words a possible 100 protein–protein complexes. Each of these 100 combinations of starting conformations was used ten times, thus generating 1000 rigid-body docking solutions. The best 200 structures after rigid-body docking, sorted according to the intermolecular energy (sum of the van der Waals, electrostatic and AIR energy terms), were subjected to semi-flexible simulated annealing (SA) in torsional space. In the final step, the structures obtained after the semi-flexible simulated annealing were refined in an explicit 8 Å water layer. The docking solutions were clustered using pairwise backbone RMSD with a cut-off of 7.5 Å and with an ensemble of at least four conformations. The ten best structures from the lowest intermolecular energy cluster were selected for manual analysis. Intermolecular contacts (hydrogen bonds and nonbonded contacts) ware analyzed with DIMPLOT, which is part of the LIGPLOT [49] software package, using the default settings (heavy-atom distance cut-off for nonbonded contacts: 3.9 Å; proton–acceptor and donor–acceptor distance cut-offs: 2.7 and 3.35 Å, respectively; minimum angle [D–H–A, H–A–AA, D–A–AA] for hydrogen bonds: 90°).

Alanine scanning mutagenesis

The amino acid residues of YsxC that interacted with L17, S2 and S10 proteins were mutated to alanine [50] using the Build Mutants protocol of Discovery Studio 2.0 [51]. Ten structure mutants were generated without applying any additional restraints. The mutant structures were used for HADDOCK docking with L17, S2 and S10 by applying the abovementioned protocol.

Molecular dynamics simulations of protein–protein complexes

The best protein–protein bimolecular complexes obtained from protein–protein interaction studies of YsxC–L17, YsxC–S2 and YsxC–S10 were subjected to MDS using the previously defined parameters for a 1 ns (1000 ps) production MD run. The lowest potential energy conformations were selected from the 1 ns MDS trajectory and further refined by energy minimization. All of the analysis was done using programs included in the GROMACS package. All of the computation was performed using Intel Core 2 Duo processors running at 2.0 GHz on an openSUSE 11.2 Linux-based operating system.

Results and discussion

Structural analysis of the homology models

Homology modeling develops a three-dimensional model from a protein sequence based on the structures of homologous proteins. A sequence identity of >45% between target and template sequence ensures the quality of the modeled protein. The alignment of the sequence with the template is displayed in Fig. 1, which gives information about sequence conservation and signature motifs.

Structural analysis of YsxC

YsxC contains several conserved motifs that are similar to those of its orthologs, YihA and YsxC of *E. coli* and *Bacillus subtilis*, respectively. An NCBI CD search reveals that from the N terminal to C terminal regions, there are two switch regions, five box motifs, and one GTP/Mg^{2+} binding site that is conserved throughout the YihA (EngB) subfamily. The G1 box motif, also known as the P-loop and the Walker A motif (GRSNVGKS, 32–39), is a motif of the

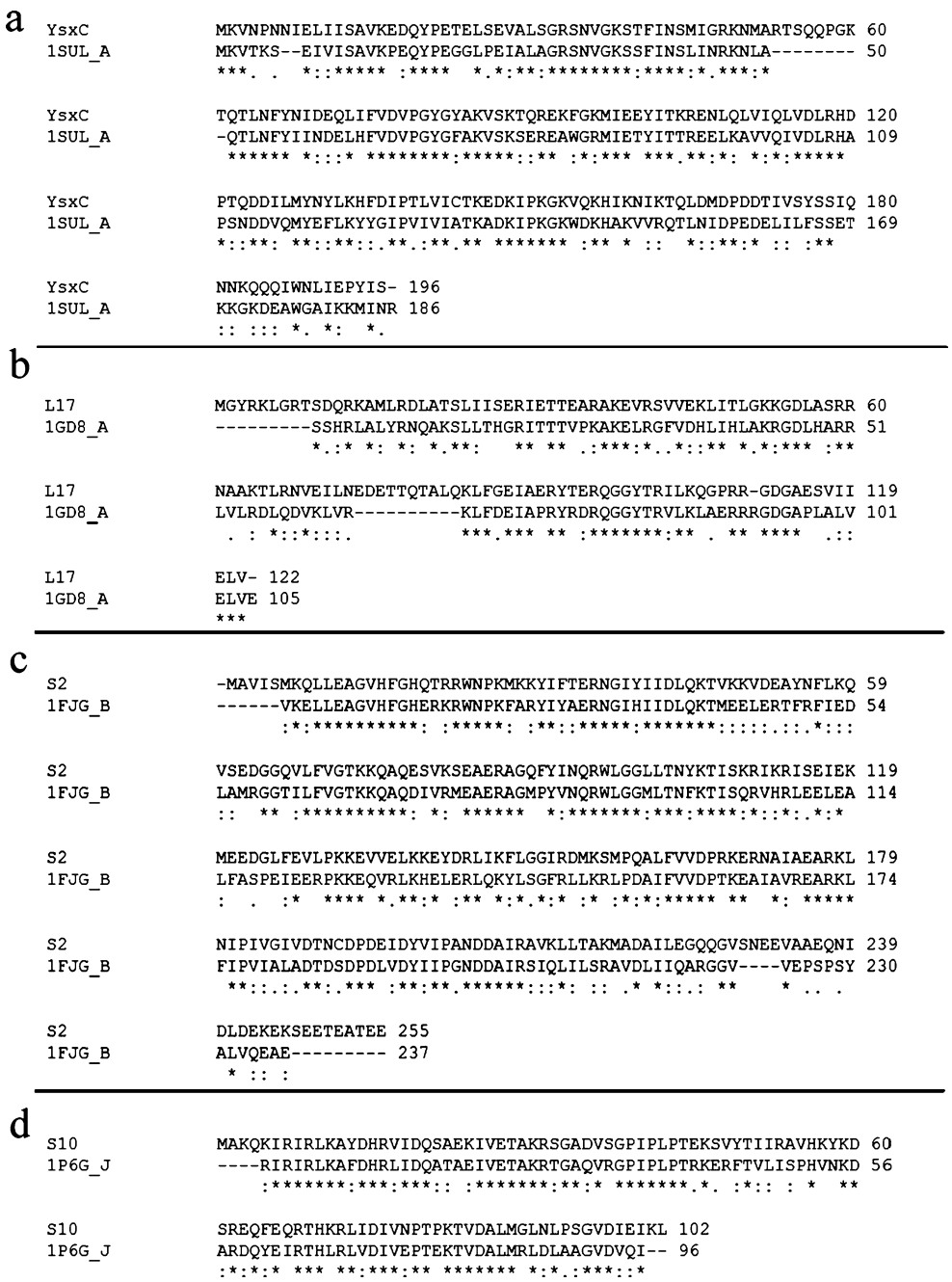

Fig. 1 **a**–**d** Pairwise sequence alignment represented by ClustalW2. **a** YsxC from *Staphylococcus aureus* and the template PDB ID: 1SUL from *E. coli*. **b** L17 from *S. aureus* and the template PDB ID: 1GD8 from *E. coli.* **c** S2 from *S. aureus* and the template PDB ID: 1FJG from *E. coli*. **d** S10 from *S. aureus* and the template PDB ID: 1P6G from *E. coli*. Symbols used in the ClustalW program: *asterisks* positions that have a single fully conserved residue, *colons* "strong" groups that are fully conserved, *periods* "weaker" groups that are fully conserved

phosphate-binding loop. The G2 box motif (52–64) overlaps with the switch I region and contains the T59 residue (responsible for interacting with magnesium), which is also conserved throughout the family. The G3 box motif (DVPG, 75–80) overlaps with the switch II region, and the G4 box motif (TKED, 140–149) is also present in the sequence alignment. In the β-turn G5 box motif (176–178), the F in the template structure is replaced by a Y residue [17]. The GTP/Mg^{2+} binding site residues S34–S39, D77, K145, D147, S177 and S178 are mapped with the target sequence, while T54, S55, Q56, G59, K60 and T61 are not aligned with the template. The structural motifs of YsxC are elucidated in Fig. 2a.

Structural analysis of L17

L17 is a member of the Ribosomal_L17 superfamily, and it contains six helices consisting of 3–17 residues and one antiparallel β-sheet (Fig. 2b). A β-hairpin loop of the 9:11 hairpin class with the conserved residues TRILK————————SVIIEL was also present in the aligned sequences. In addition, 11 β-turns, two γ-turns

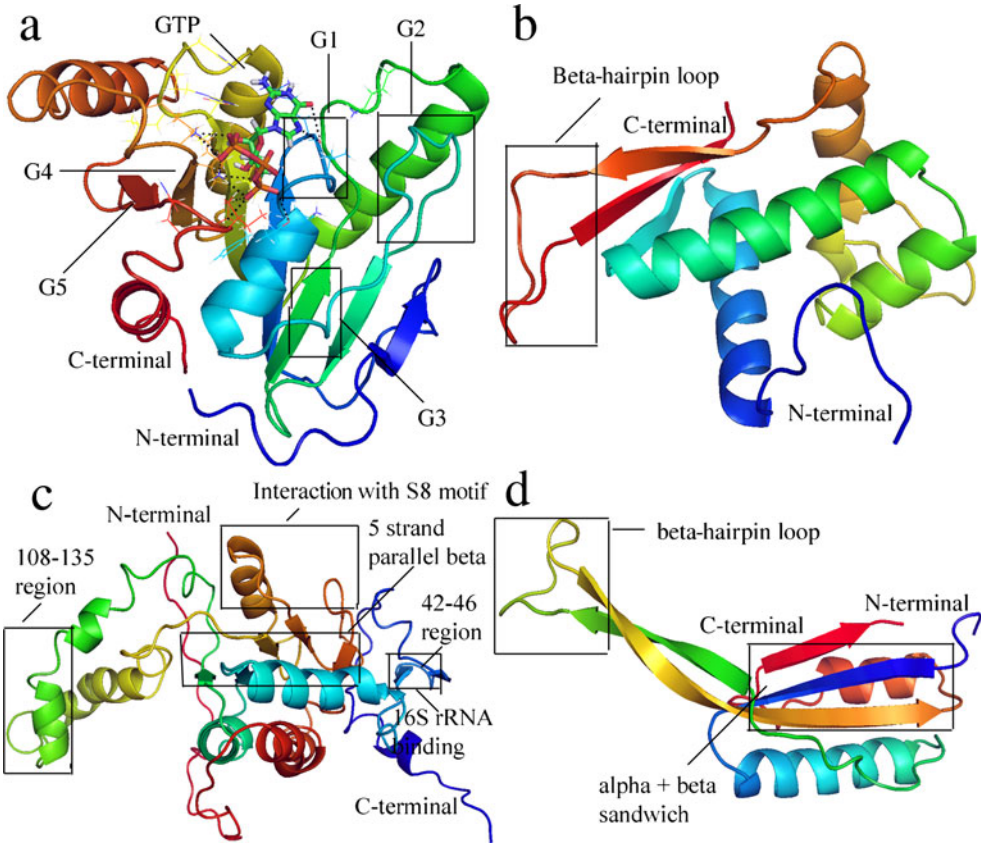

Fig. 2 a–d The three-dimensional structures of homology models. **a** YsxC. The structural motifs G1, G2, G3, G4 and G5 are labeled with *boxes*. The GTP-binding residues of YsxC are displayed as *lines*, whereas GTP is displayed as *sticks*. **b** L17. A β-hairpin loop (in the *box*) is the highly flexible region. **c** S2. Structural motifs such as the 16S rRNA binding motif, the five-stranded parallel β, the interaction with S8, the 42–46 region, and the 108–135 region are labeled with *boxes*. **d** S10. This contains an α + β sandwich motif and a β-hairpin loop. For all proteins, *blue* indicates an N terminus and *red* a C terminus. The figures were prepared using PyMol

and six helix–helix interaction motifs were also maintained throughout the target–template sequence alignment.

Structural analysis of S2

Sequence analysis and an NCBI CD search showed the presence of two structural motifs in the S2 protein. The modeled structure of the S2 protein is displayed in Fig. 2c. The first motif is responsible for interacting with 16S rRNA (especially in the region 34–36) [52], while the second motif (R177, K178, N180, D194, E195, I196 and D197) interacts with ribosomal protein S8 in the 30S subunit of the ribosome. The 30S ribosomal protein S10 is predicted to be the functional partner of S2, which is involved in the binding of tRNA to the ribosome. The secondary structural information reveals the presence of six strands, ten helices, one β-hairpin, two β-bulges, and two γ-turns throughout the structure. Nest analysis reveals the presence of three nests, A87–Q89, G99–L101 and L179–I181, with a maximum cleft depth of 17.74, which strongly indicates that it is functionally important (nests are structural motifs that are often found in functionally important regions of protein structures).

Structural analysis of S10

S10 is a member of the Ribosomal_S10 superfamily, and it was modeled with 80% similarity using its template 1P6G. S10 consists of two helices packed against a four-stranded sheet to form a small α + β sandwich domain with a so-called double-split β-α-β fold (Fig. 2d). The two central β-sheets connected by a long β-hairpin loop may penetrate deeply into the center of the RNA, as in the S10 protein of *Thermus thermophilus* [52], which is indicated by structural analysis and the conservation of sequence between both S10 proteins.

Analysis of the stability of modeled structures by MDS and ED (essential dynamics)

In order to evaluate the stability of the homology models, molecular dynamic calculations were carried out for 3 ns. The minimum and maximum potential energies of YsxC, L17, S2 and S10 are listed in Table 1, which shows that all of the models were energetically stable during the production MD simulation. The RMSD profiles of each protein are described in Fig. 3a, which shows that the RMSD trajectory of YsxC rises during the first 200 ps (the equilibration period) and remains quite stable during the following period, with an average RMSD of 0.15 nm, whereas L17, S2 and S10 stabilized after equilibration periods of 1500 ps, 1800 ps and 1200 ps with average RMSD asset values of 0.45, 0.75 and 0.55 nm, respectively. The lowest potential energy of each protein trajectory was selected and retrieved for Ramachandran plot, ERRAT score and Verify3D

Table 1 Results of molecular dynamics studies carried out on the proteins L17, S2, and S10

Protein	YsxC	L17	S2	S10
RMSD profile (from 3 ns MD trajectory)				
Equilibration period (ps)	200	1500	1800	1200
RMSD (nm)	0.15	0.45	0.75	0.55
Potential energy (kJ/mol)				
Maximum PE	−527000	−557000	−1312000	−974500
Minimum PE	−531000	−561000	−1319000	−980800
Ramachandran plot assessment				
Residues in favored region (%)	85.3	83.5	79.2	90
Residues in additionally allowed region (%)	12.4	14.7	19	8.9
Residues in generously allowed region (%)	1.7	0.9	1.3	1.1
Residues in disallowed region (%)	0.6	0.9	0.4	0
Verify_3D score	96.45	86.99	88.13	75.73
ERRAT score	94.25	97	86.66	79.71

analysis, which showed that all models had good quality factors and were reliable (Table 1) for further studies. The overall atomic fluctuation of each protein during the 3 ns timescale of the MD simulation was also calculated and is described in Fig. 3b–e for YsxC, L17, S2 and S10, respectively. These results indicate that the YsxC proteins have three flexible motifs called G2 (52–60), a switch II region overlapping with G3 (75–80), and a 170–175 region overlapping with the G5 motif with RMSF values ranging from ~0.1 to 0.25 nm. In the case of the L17 protein, one turn (70–85) and a β-hairpin loop (105–115) fluctuate by ~0.15 to 0.30 nm, whereas turn1 (16S rRNA binding, the 42–46 region) and turn2 (108–135) of the S2 proteins fluctuate more, with RMSF values ranging from ~0.2 to 0.4 nm. In S10 proteins, the β-hairpin loop region (48–70) shows even more fluctuation, with RMSF values ranging from ~0.3 to 0.68 nm. All of these results indicate that the abovementioned flexible regions of each protein play important roles in the interactions with the protein's interaction partners by maintaining the conformational changes during the 3 ns MD.

PCA analyses of YsxC, L17, S2 and S10 were calculated and diagonalized based on a trajectory of 1501 frames with covariance matrix dimensions of 1764 for YsxC, 1098 for L17, 2295 for S2 and 918 for S10. These dimensions were given by 588 backbone elements for YsxC, 366 for L17, 765 for S2, and 306 for S10, with eigenvalue sums of 4.61468, 12.2082, 70.4893 and 16.1925 nm^2, respectively. Plotting eigenvalues against the eigenvectors of each protein yielded steep eigenvalue curves (see Fig. 3f), and it was noted that 90% of the backbone motion is covered by the first 20 eigenvectors. These results indicate that the most of the internal motion of the proteins is restricted to a subspace with very small dimensions. A more accurate analysis of the motion along the eigenvector direction was obtained by projecting the trajectory onto these individual eigenvectors. Figures 4a, c, e and g show the first three, the tenth and the twentieth projections of the backbone trajectory onto the eigenvectors gained from the backbone covariance matrix and plotted against time for each of YsxC, L17, S2 and S10 for the 3 ns of simulation, respectively. These results indicate that the motions of the backbone reached their equilibrium fluctuations in the first ten eigenvectors. Figures 4b, d, f and h show the trajectory projected onto the planes defined by two eigenvectors (the tenth and twentieth eigenvectors) from the backbone coordinate covariance matrix for YsxC, L17, S2, and S10, respectively. These two eigenvector projections onto the plane of the backbone motion of each protein are strongly correlated, and fill the expected ranges almost completely. The results indicate that the sets are similar and there is no high projection observed far from the diagonal. Then, superposition analysis of the average structure calculated using the backbone covariance matrix with the native structure shows RMS deviations of 0.612, 0.900, 1.951, and 0.912 for YsxC, L17, S2, and S10, respectively. The results obtained indicate that the modeled structures show prolonged stability in the timescale of the 3 ns MD simulation, which in turn favors the selection of these structures for further analysis.

Binding site analysis of YsxC

The binding site of YsxC was predicted using the PSiFR and Q-SiteFinder servers, which actually yielded identical pairs of binding pockets. The first site was the GTP-binding site with a volume of 482 $Å^3$; the residues that formed the cavity (with high probability scores) were S34, G37, T40, S55, K60, K145, D147, S177, and S178. Another binding cavity with a volume of 424 $Å^3$ was ranked next to this site, and was located close to the GTP-binding site. This arrangement suggests the possibility of introducing struc-

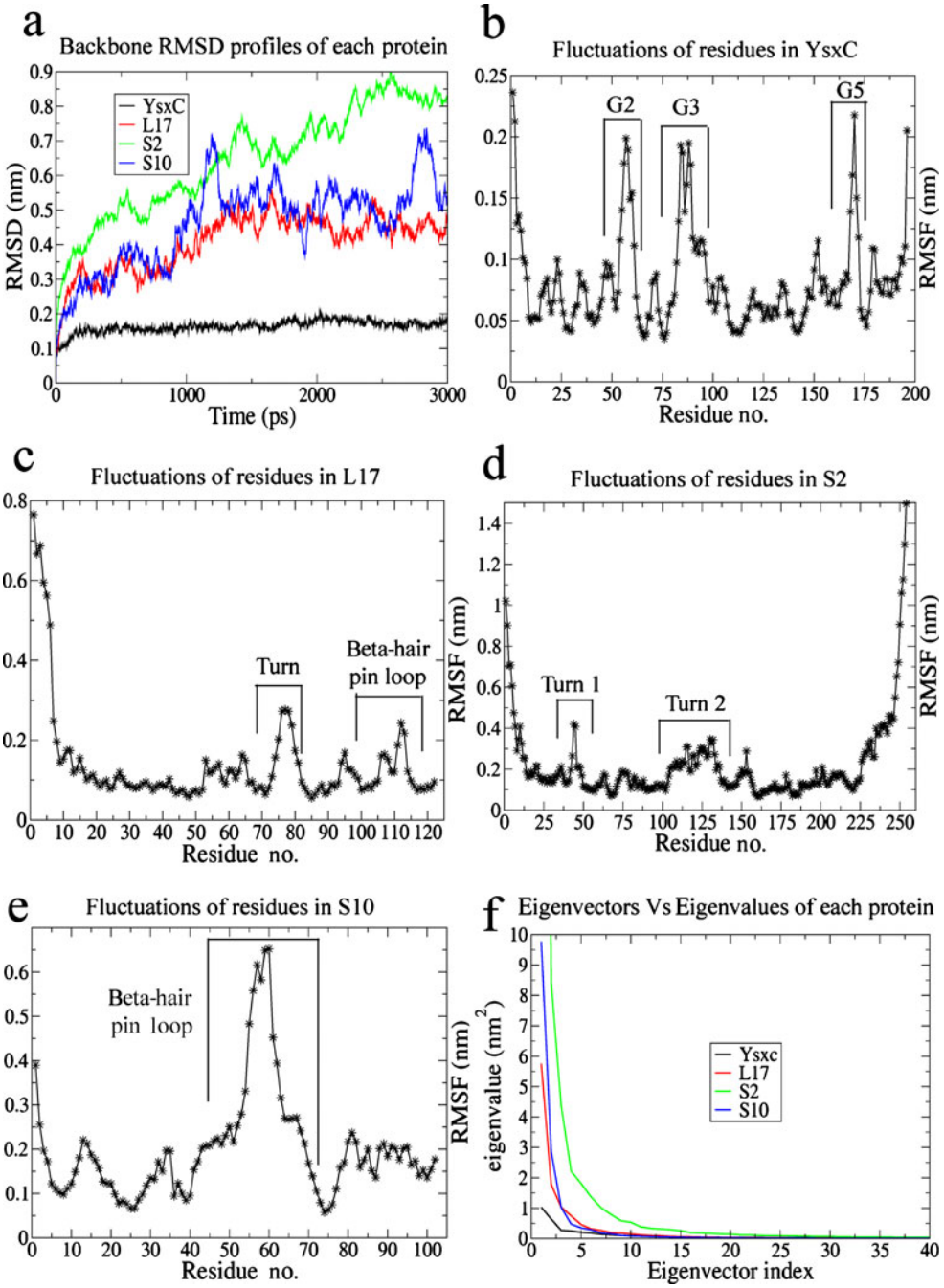

Fig. 3 **a**–**f** Stability analyses of structures modeled by MDS and ED. **a** The backbone RMSD profiles for YsxC, L17, S2 and S10 are plotted against the 3 ns MD simulation: *black* YsxC, *red* L17, *green* S2, *blue* S10. **b** The RMS fluctuations of residues in YsxC: structural motifs like G2, G3 and G5 are shown to be among the most flexible regions. **c** L17: a turn and β-hairpin loop are shown to be the most flexible regions, **d** S2: turn1 (16S rRNA binding region) and turn2 (108–135) are shown to be the most flexible residues. **e** S10: the β-hairpin loop (48–70) is the most flexible region. **f** Eigenvalues for YsxC, L17, S2 and S10, shown in decreasing order of magnitude and obtained from the backbone coordinate covariance matrix as a function of the eigenvector index. All of the graphs were plotted using xmgrace, a 2D plotting tool

tural changes at the GTP-binding site by altering the conformation of residues in this second binding cavity. Conversely, the C-terminal region of *B. subtilis* YsxC [17] was found to have an allosteric effect on its function. Accordingly, we analyzed for the possibility of utilizing the same region of *S. aureus* to introduce allosteric effects, but huge sequence differences between these sites in YsxC of *S. aureus* and YsxC of *B. subtilis* prevented us from using this site for allosteric inhibition studies. Due to its close proximity to the substrate-binding site, the binding of the ligand in this pocket may affect the affinity of substrate binding. Moreover, the residues in this pocket were found to represent the most flexible region of the YsxC protein, next to the GTP-binding region, via 3 ns MD simulation. Thus, the binding cavity next to the GTP-binding site (S31, Y81, Y83, R91, G95, I98, Y101, L114, M128 and Y131) was selected for the analysis of allosteric inhibition.

Molecular docking analysis

In order to determine the GTPase activity of the YsxC protein, the substrate GTP was selected for interaction studies at the active site, while the selected ligands were docked at the allosteric site for allosteric inhibition.

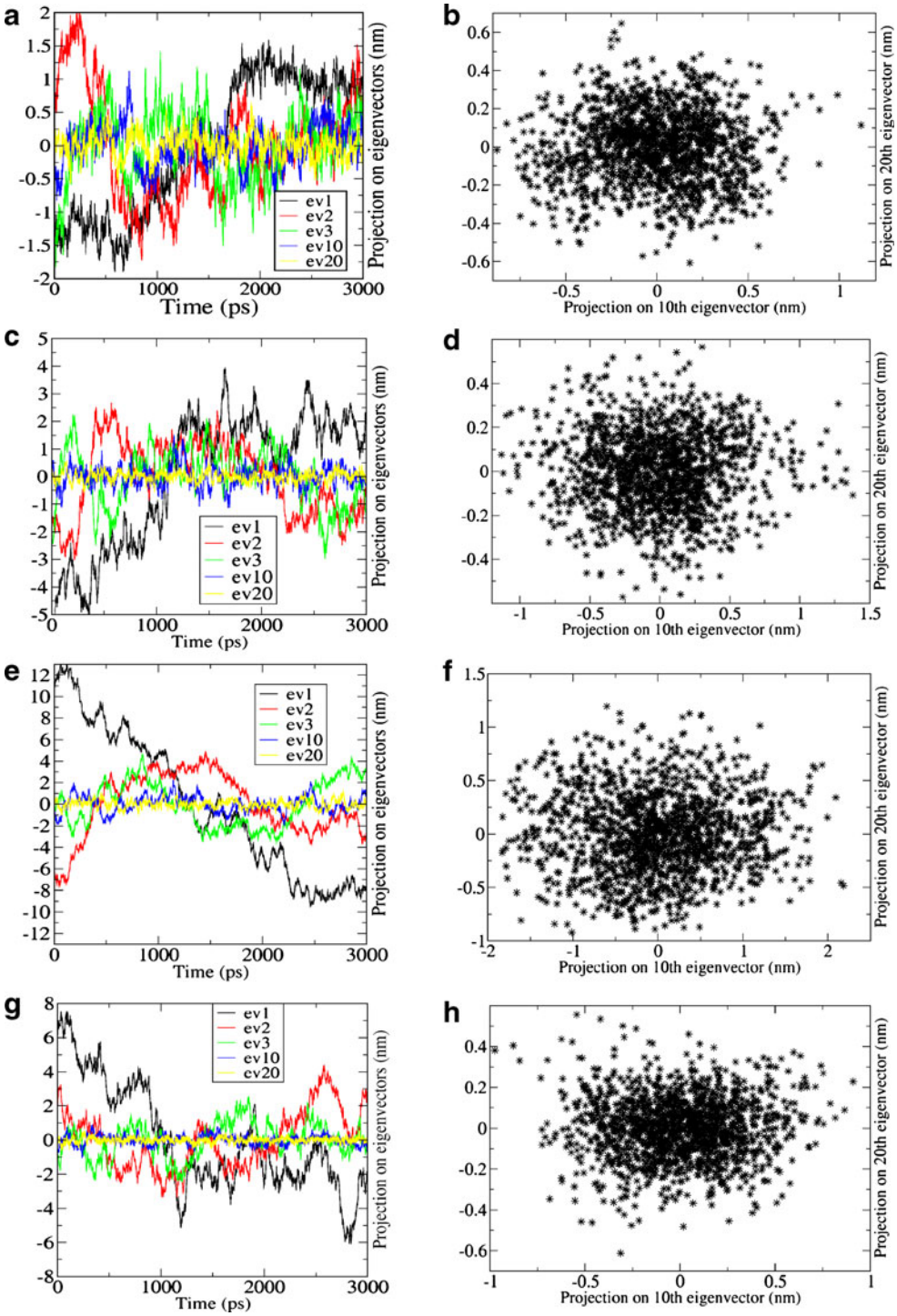

Fig. 4 **a**–**g** Motion and projection of trajectory by ED analysis. **a**, **c**, **e** and **d** shows the motions along the first three, the tenth and the twentieth eigenvectors obtained from the backbone coordinate covariance matrix for YsxC, L17, S2, and S10, respectively. **b**, **d**, **f** and **g** are the projections of the trajectory onto the planes defined by the tenth and twentieth eigenvectors from the backbone coordinate covariance matrix for YsxC, L17, S2, and S10, respectively

Interactions of GTP at the active site

The two-dimensional molecular structure of GTP is displayed in Fig. 5. The simulation of the docking of GTP with YsxC provides insight into the binding affinity and mode of interaction of GTP at the active site, which has a Glide score of −10.61. A very low Emodel score (−107.97) also suggested an energetically favorable interaction of GTP at the active site. The binding mode of GTP at the active site of YsxC involves hydrogen-bonding interactions (see Fig. 7a) with eight amino acid residues: S34, T40, D116, D144, K145, S178, I179 and Q180. In addition, the presence of van der Waal (vdW) interactions with the residues V36, G37, F41, K148, and Y176 provides further stability to the complex. The protein–substrate complex was subjected to MDS in order to check the sustainability of GTP at the active site of the protein.

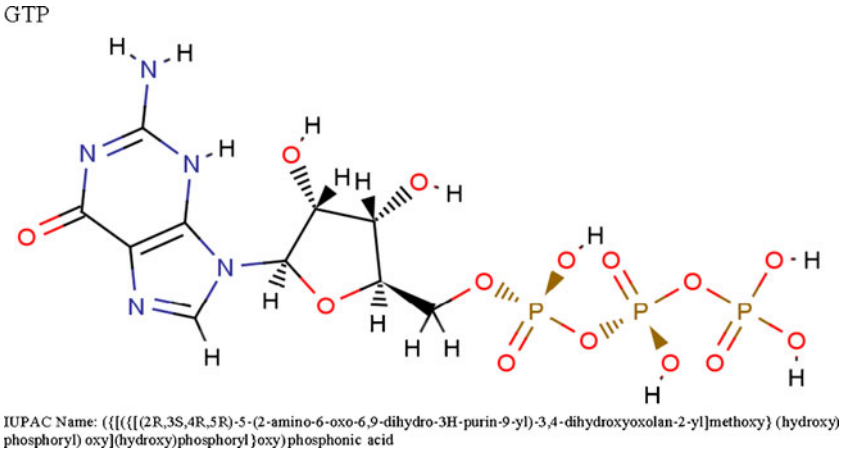

Fig. 5 Two-dimensional molecular structure of the natural substrate GTP of the protein YsxC, along with its IUPAC name. The figure was prepared using MarvinView 5.1.1

Interactions of ligands at the allosteric site

Among a library of 10,230 ligands, only six potential hits were identified for the comprehensive interaction analysis focusing on the allosteric site of YsxC. These six were selected based on their interaction modes and the high energy scores of each ligand with YsxC. The two-dimensional molecular structures of these ligands are displayed in Fig. 6. Docking simulations of all six ligands with YsxC indicated that they all exhibited a hydrogen-bonding interaction with R91 (NH1, NH2 and NE atoms), vdW interactions with Y81, Y83, R91, D124 and Y131, and a C–H–π interaction with Y131. Other than the abovementioned interactions, each ligand presented other hydrogen bonds and vdW interactions with YsxC, as described in the following. Ligand 1 forms a hydrogen bond with D124 and also vdW interactions with I98, E99, I102 and L127, yielding a Glide docking score of −9.84 (Figs. 7 and 8a). The docked complex of Ligand 2–YsxC shows that Ligand 2 binds at the allosteric site through

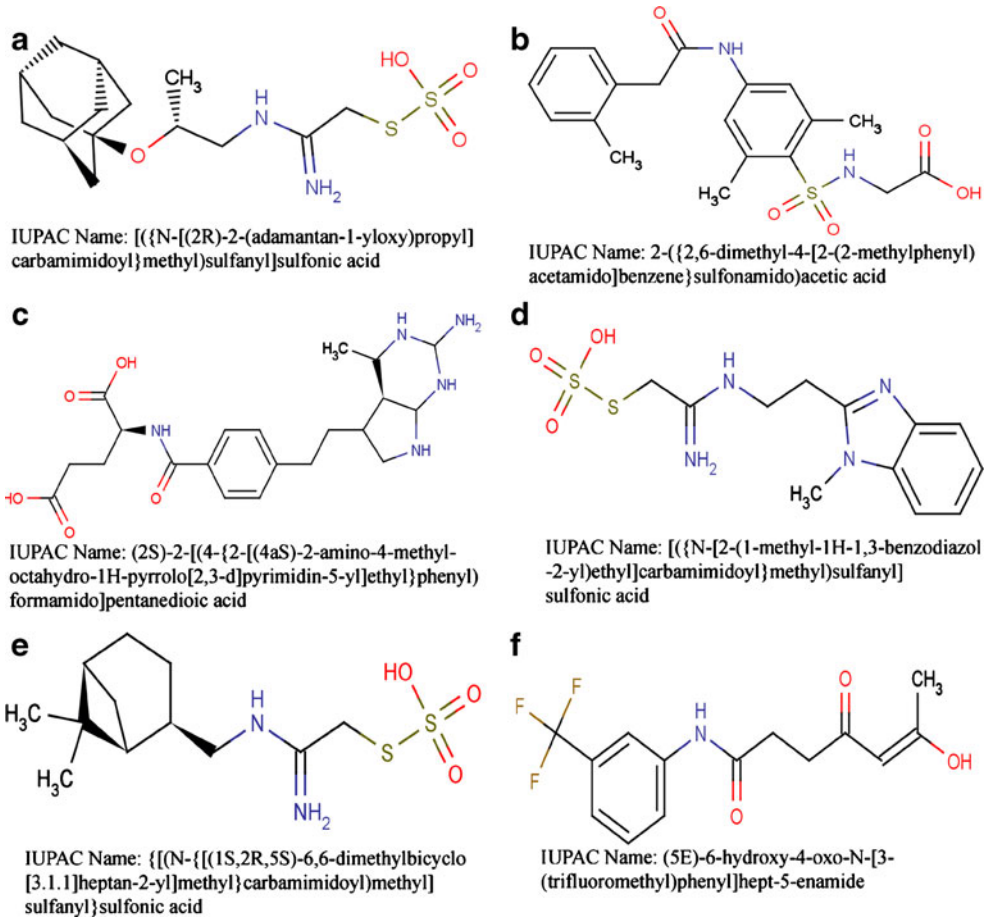

Fig. 6 Two-dimensional molecular structures of the best six ligands selected after docking studies, along with their IUPAC names. The figures were prepared using MarvinView 5.1.1

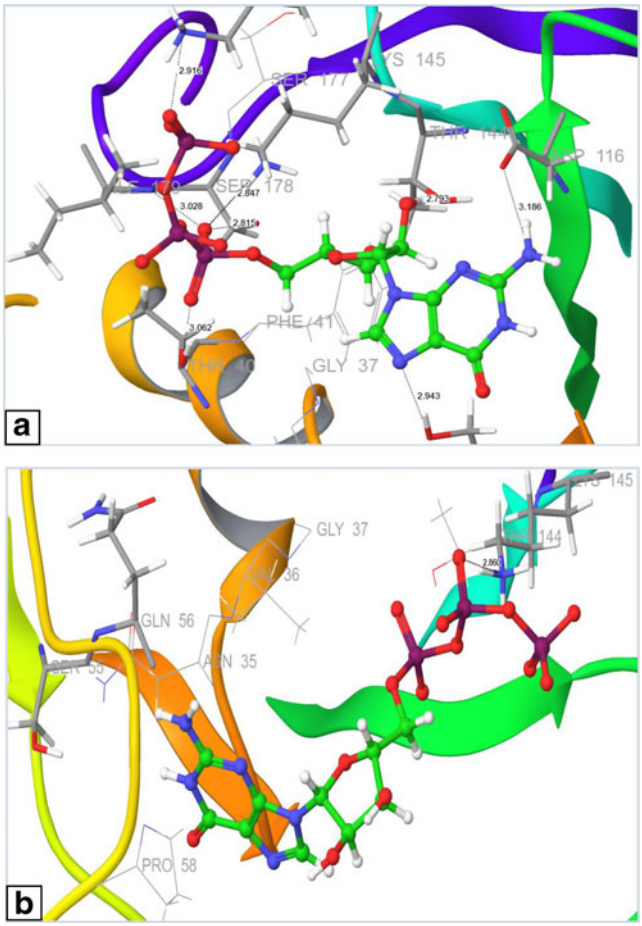

Fig. 7 **a**–**b** Docking modes of GTP at the binding sites of YsxC. **a** GTP binding at the active site. **b** Allosteric inhibition of YsxC in the form of a reduced binding affinity at the active site. The hydrogen-bonding residues are shown as *sticks* and are colored by atom type: hydrogen is colored *white*, carbon is *gray*, oxygen is *red*, nitrogen is *blue*, sulfur is *yellow*, and phosphorus is *violet*. The residues involved in van der Waal interactions are shown in *wire-frame form*. Ligands are shown as *ball-and-stick drawings with green-colored carbon atoms*

hydrogen bonds with K88 and Y81 and vdW interactions with A84, K88, I98, E99 and M128, giving a Glide docking score of −9.48 (Fig. 8b). The interacting conformation of Ligand 3 with YsxC (which has a docking score of −9.46) reveals the presence of hydrogen bonds with K88, E99 and Y83, and vdW interactions with K85, K88, I98, E99 and M128 (Fig. 8c). The interaction of Ligand 4 with YsxC was stabilized through the formation of hydrogen bonds with Y83 and D124, and vdW interactions with A84, I98, I102 and M128, leading to a Glide docking score of −9.44 (Fig. 8d). Hydrogen bonding with D124 and vdW interactions with A84, K88, I98 and L127 allow Ligand 5 to fit into the allosteric site of YsxC with a docking score of −9.19 (Fig. 8e). Moreover, in the Ligand 6–YsxC complex, the ligand hydrogen bonds with the residues Y83 and Y81 and presents vdW interactions with A84, K88, E99 and L127, producing a Glide score of −9.16 (Fig. 8f). The aromatic ring of each ligand shows a C–H–π interaction with Y131, which also participates in the stabilization of these ligands in the allosteric cavity. The hydrogen bond donors, acceptors, H-bond lengths, residues involved in vdW interactions, Glide docking scores, and Glide Emodel scores of the ligands with YsxC are listed in Table 2. In summary, the docked conformations of each ligand with YsxC provide insight into the possibility of a mechanism for inhibiting the function of YsxC, and thereby suppressing the growth of *S. aureus*. The differences in the Glide docking scores and Emodel scores are very small among all six ligands. However, finally, the YsxC–Ligand 3 conformation—which has the lowest Glide Emodel score—was selected for further analysis of the influence of this ligand on the binding of GTP.

Interaction of GTP in the presence of Ligand 3

The protein conformation obtained from the induced fit docking of YsxC and Ligand 3 was used to investigate how the substrate (GTP) binding is affected by the presence of the ligand at the allosteric site. The results of this analysis (Fig. 7b) reveal that there is a low binding affinity of GTP to YsxC in the presence of Ligand 3, which is confirmed by the Glide docking score of −4.58 and Emodel score of −52.6. Interactions of backbone oxygen atoms from both S55 and Q56 with the amine group of the adenine ring result in the formation of two hydrogen bonds, whereas the side-chain nitrogen atom in K145 hydrogen bonds to the oxygen atom of the second phosphate group of GTP. vdW interactions with the residues N35, V36, G37, P58, K85 and T144 provide some stability to the complex. The amino acid residues S34, T40, S177 and S178, which are involved in the binding to GTP in the absence of other ligands, are not able to interact with GTP when Ligand 3 is bound to YsxC. The results obtained from the docking studies suggest that the binding of ligands at the allosteric site may inhibit substrate binding at the active site. This is because the natural substrate of YsxC (GTP) is only loosely bound to the active site due to conformational changes in the protein; this may inhibit ribosome assembly and thereby suppress the growth of *S. aureus*.

MD analysis of the YsxC–GTP complex in the presence and absence of Ligand 3 at the allosteric site

Figures 9a and c show the variation in the RMSD of the backbone of the YsxC–GTP complex as the simulation proceeds in the cases of substrate binding and allosteric inhibition, respectively. Interestingly, in the case of substrate binding, the RMSD of the YsxC protein remains below 0.175 nm during the first 1000 ps; it then reaches

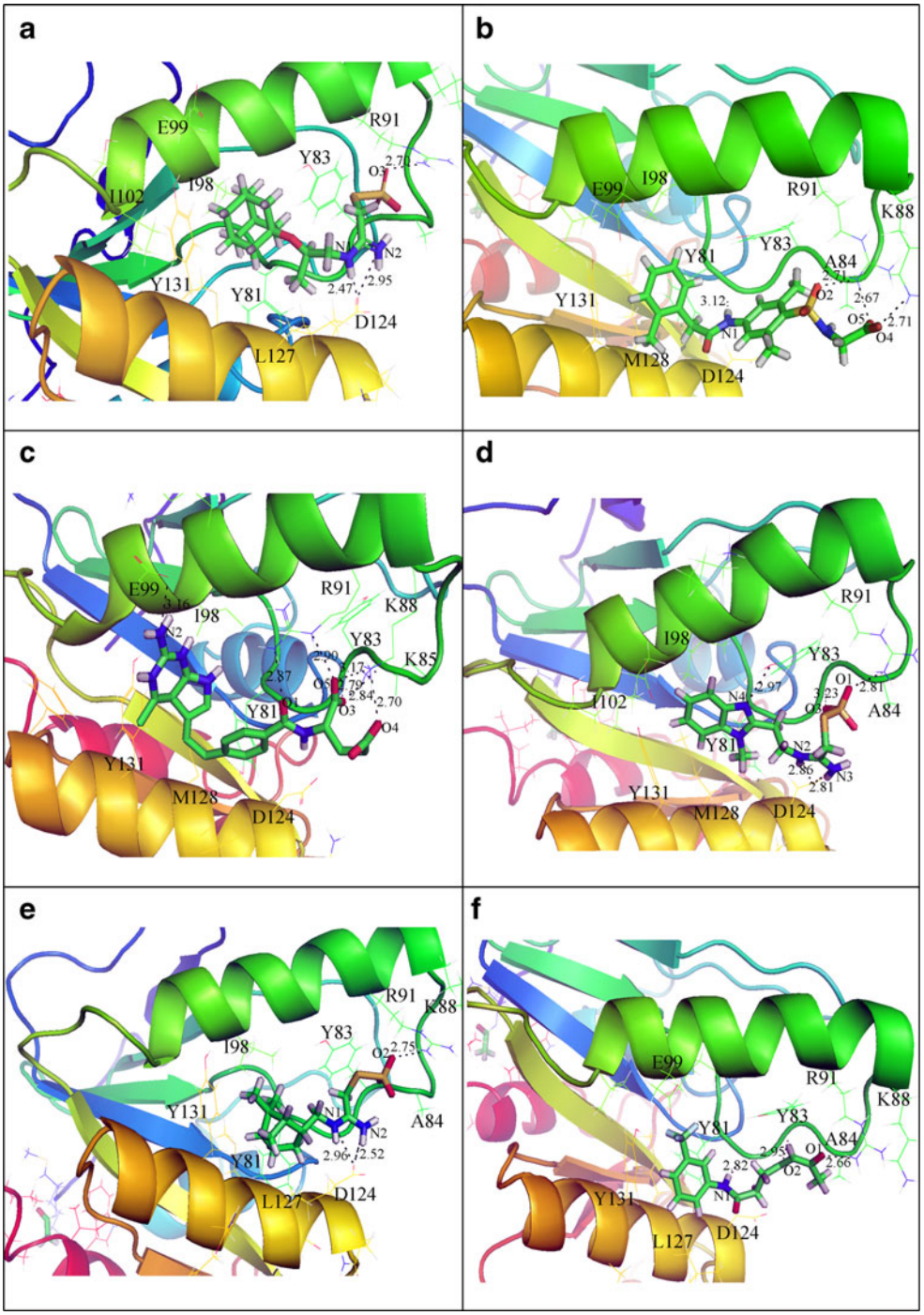

Fig. 8 **a**–**f** Docking modes of the best six ligands with YsxC. Interactions of YsxC with: **a** Ligand 1, **b** Ligand 2, **c** Ligand 3, **d** Ligand 4, **e** Ligand 5, **f** Ligand 6. The hydrogen-bonding residues and those involved in vdW interactions are shown as l*ines*. The hydrogen-bonding interactions are shown as *black dotted lines*, and the distances between the atoms involved are given. The ligands are shown as *ball-and-stick representations with green-colored carbon atoms*

~0.2 nm in the next 200 ps, before it stabilizes at ~0.22 nm for the rest of the simulation. This indicates that when the YsxC is in complex with GTP, the conformation changes at around 1200 ps. When Ligand 3 binds at the allosteric site, the RMSD of YsxC shows a gradual change with a maximum deviation of 0.4 nm from the starting conformation. This result indicates that the conformation of the YsxC–GTP–Ligand 3 complex does not stabilize completely during the 3 ns MD simulation. When the substrate binds to YsxC, hydrogen bonds at the backbone of the protein structure control the switch in conformation. Accordingly, we monitored the lengths of the hydrogen bonds formed between the residues K145, K148 and I179 and Ligand 3 during the 3 ns of simulation, and this interaction profile is displayed in Fig. 9b. The backbone nitrogen atom of I179 forms a hydrogen bond with the O7 atom of GTP during the period 100–1200 ps. Afterwards, a hydrogen bond is observed from 1200 ps to 3000 ps between O6 of GTP and N of Ile179. This H-bond profile exactly matches the RMSD of the protein backbone, which reflects conforma-

Table 2 Molecular interactions of the six ligands at the allosteric site of YsxC

Molecules	Hydrogen-bonding interaction			Residues involved in vdW interactions (scaling factor = 1.00 Å)	Glide docking score	Glide Emodel score
	H-bond donor	H-bond acceptor	H-bond length (A)			
Ligand 1	Lig:: N1	D124: OD1	2.47	Y81, Y83, R91, I98, E99, I102, D124, L127 and Y131	−9.84	−50.29
	Lig:: N2	D124: OD1	2.95			
	R91: NH1	Lig:: O3	2.70			
Ligand 2	Lig:: N1	Y81: O	3.12	Y81, Y83, A84, K88, R91, I98, E99, D124, M128 and Y131	−9.48	−55.09
	K88: NZ	Lig:: O4	2.71			
	R91: NH1	Lig:: O5	2.67			
	R91: NH1	Lig:: O2	2.71			
Ligand 3	Lig:: N2	E99 : OE2	3.16	Y81, Y83, K85, K88, R91, I98, E99, D124, M128 and Y131	−9.46	−72.41
	K88: NZ	Lig:: O4	2.70			
	K88: NZ	Lig:: O5	2.79			
	R91: NE	Lig:: O5	2.87			
	R91 : NH2	Lig:: O1	2.90			
	Y83 : N	Lig:: O3	3.17			
Ligand 4	Y83: N	Lig:: O2	3.23	Y81, Y83, A84, R91, I98, I102, D124, M128 and Y131	−9.44	−50.12
	R91: NH1	Lig:: O1	2.81			
	Lig:: N2	D124: OD1	2.86			
	Lig:: N3	D124: OD1	2.61			
	Lig:: N4	Y83: OH	2.97			
Ligand 5	R91: NH1	Lig:: O2	2.75	Y81, Y83, A84, K88, R91, I98, D124, L127 and Y131	−9.19	−42.64
	Lig:: N1	D124: O3	2.96			
	Lig:: N2	D124: O3	2.52			
Ligand 6	Y83: N	Lig:: O2	2.95	Y81, Y83, A84, K88, R91, E99, D124, L127 and Y131	−9.16	−49.26
	R91: NH1	Lig:: O1	2.66			
	Lig:: N1	Y81: O	2.82			

tional changes at the active site. Similarly, the side-chain nitrogen atoms of both K145 and K148 form two H-bonds with the oxygen atom (O14) of GTP throughout the simulation period, and provides stability to the complex. The YsxC–GTP complex has a stable conformation throughout the simulation, with a potential energy of about -5.48×10^5 kJ mol^{-1}. Thus, the three residues mentioned above are all considered to be crucial to substrate binding.

In the case of the YsxC–Ligand 3–GTP complex, the gradual change in the RMSD of the protein backbone and the increase in the potential energy of the system show that the YsxC–GTP complex is less stable in the presence of Ligand 3 at the allosteric site. The hydrogen-bond profile (Fig. 9d) shows that the side-chain nitrogen atom of K145 forms an H-bond with O11 of GTP during the period 0–1.7 ns (aside from 1.2–1.4 ns); however, the H-bond is broken from 1.7 to 2.3 ns. After that, the H-bond is reactivated. Similarly, backbone O atoms of both S55 and Q56 form H-bonds with the nitrogen atom of GTP. Changes in the H-bond profile of Lys145 may be responsible for the changes in the RMSD profile, as it is one of the main residues involved in the binding of GTP to YsxC in the absence of ligand binding at the allosteric site, while the other two residues (K148 and I179) are not involved in any interaction. Thus, interaction analysis of the YsxC–GTP complex under both conditions supports our hypothesis of allosteric inhibition of substrate binding.

MD analysis of YsxC in complex with Ligand 3 at the allosteric site

MD analysis of the stability of the YsxC–Ligand 3 complex during the simulation was facilitated by monitoring the RMSD profiles computed from the atomic displacements during the MD trajectory. Figure 9e shows that the RMSD rises during the first 1600 ps to ~0.25 nm, and then remains quite stable during the rest of the simulation. The initial increase in the RMSD can be seen as a fluctuation in the H-bonds between ligand and protein residues. The low potential energy value of -5.4×10^5 kJ mol^{-1} indicates that the complex is energetically stable during the MD simulation. The H-bond profile of the YsxC–Ligand 3 complex, as displayed in Fig. 9f, reveals that the complex is stabilized by three H-bonds. The nitrogen atoms of A84, R91 and

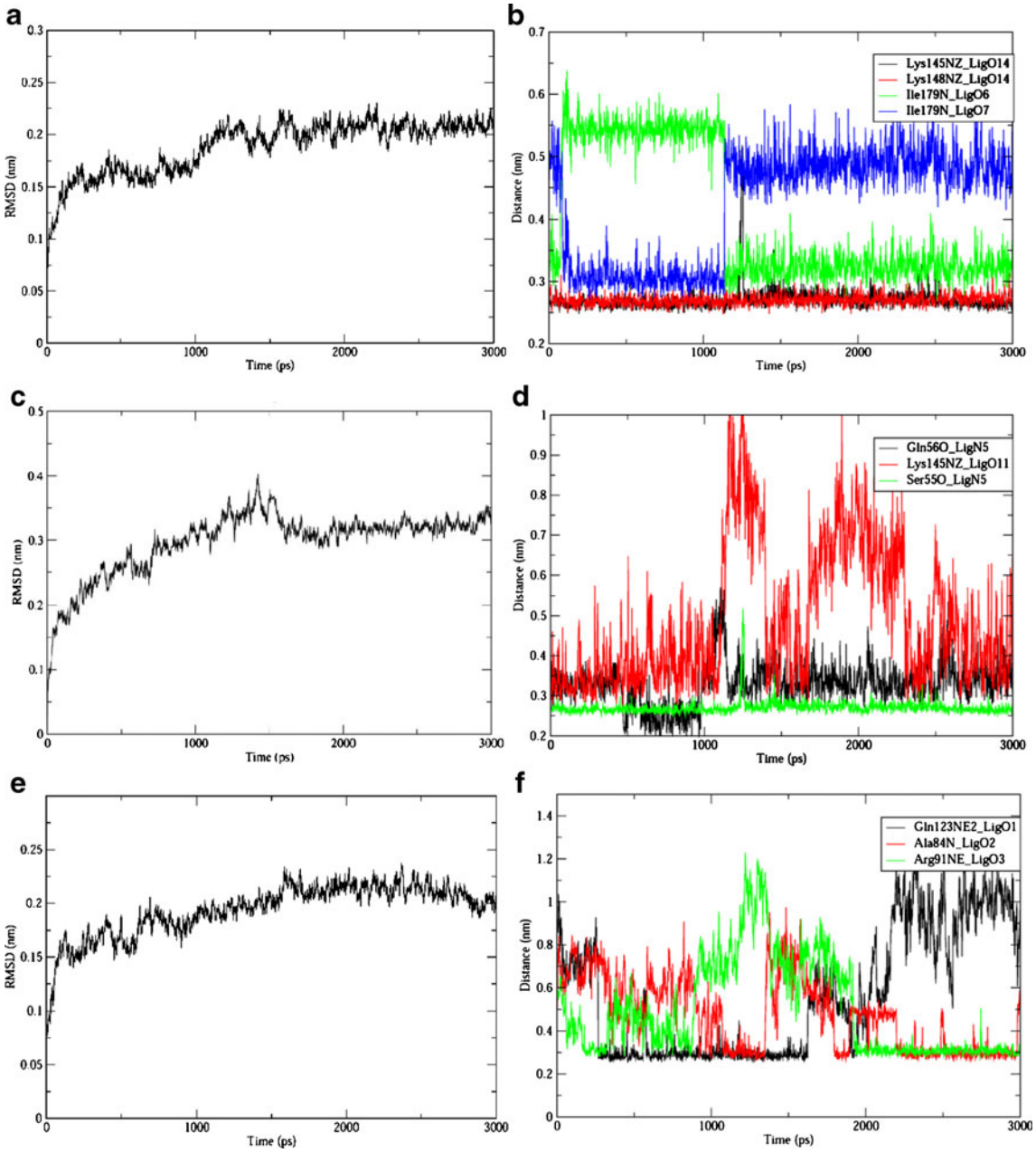

Fig. 9 **a**–**f** MD trajectory based analysis of the YsxC–GTP complex, in terms of substrate or Ligand 3 binding and allosteric inhibition. **a**, **c** and **e** show the RMSD profiles for the abovementioned complexes, while **b**, **d** and **f** show the atomic distances between the atoms involved in H-bond formation

Q123 maintain H-bonds with the O2, O3 and O1 atoms of Ligand 3 throughout the 3 ns of simulation. A small increase in the RMSD at 1600 ps was noted, which was due to the scission of the H-bond between the residue Q123 and Ligand 3, but the H-bonds involving A84 and R91 provide substantial stability throughout the simulation period. The stability of the YsxC–Ligand 3 complex provides insight into the potential antibacterial activity gained by targeting YsxC.

Predicting interface sites

Protein–protein interaction analyses are crucial to understanding many biological processes such as ribosome assembly, and so-called interaction sites or functional sites are very important in these protein–protein interactions. The calculation of accessible surface area and the interface propensity score of each amino acid provide information on the solvent-exposed residues of YsxC, L17, S2, and S10.

Based on the prediction score, the residues are grouped into active (high score) and passive (relatively low) residues for the abovementioned proteins. The predicted active and passive residues of YsxC, L17, S2 and S10 were also checked against the neural network scores predicted by the cons-PPISP and PatchDock servers. Moreover, the predicted active site residues of YsxC, L17, S2 and S10 were shown to be in the most flexible region during the 3 ns MD simulation. All of these results suggest that the predicted interface site residues can be used for further protein–protein interaction studies. A list of the active and passive interface residues for each protein along with the flexible segments is given in Table 3.

Protein–protein interaction analysis

A HADDOCK docking simulation was performed to gain structural insights into the roles of the interface residues involved in protein–protein interactions. The best 200 structures were clustered for each of YsxC–L17, YsxC–S2 and YsxC–S10, based on the intermolecular energies of the docked structures. HADDOCK analysis of the best clusters showed intermolecular energies of at least −400 kcal mol^{-1} and very low (<2 Å) RMSD deviations, suggesting that the structure of each complex is very stable. The RMSD values for the averages of the ten best structures from the lowest-energy clusters are given in Table 4. The best structure from each cluster provides the interface information for each protein–protein complex.

YsxC–L17 interactions

The YsxC–L17 complex with the lowest intermolecular energy (−782.84 kcal mol^{-1}) was selected for interaction analysis. DIMPLOT analysis of the YsxC–L17 complex (Fig. 10a) reveals that the amino acid residues R33 (from the G1 motif), S55–Q57 (G2 motif region), Y81, G82, A84, K85, K88 and R91 (switch II region), and R118, H119, D120, P121 and D124 of YsxC are involved in H-bond interactions with the residues in the N-terminal hotspots (E28, R29, E34, K38 and E45) and the C-terminal antiparallel β-sheet (T101, R102, K105, Q106, G107, E115, E120, L121 and V122) in the L17 protein. The presence of fluctuating interactions involving the residues of these complexes points to the reliability of the docking results. The buried surface area of 2218 $Å^2$ provides more interface regions for the complex. YsxC interacts with L17 and forms the large 50S subunit of the 70S ribosome. The binding affinity for this process is very high, as predicted by the docking scores, thus providing insight into the importance of YsxC to ribosomal stability. An assessment of the Ramachandran plot of the YsxC–L17 complex also reveals the strength of the complex.

YsxC–S2 interactions

The best complex structure from the YsxC–S2 cluster in terms of intermolecular energy (−552 kcal mol^{-1}) is displayed in Fig. 10b. In this structure, the residues of the N-terminal region (L10 and V15) and part of the G2 motif region (R53, S55, Q57, G59, K60 and T61) in YsxC are involved in various hydrogen-bonding and vdW interactions with the residues E116, K119, D123, F126, E127, V128, P130 and K131 of the S2 protein. In the S2 protein, residue E116 is present in an α-helix, whereas D123, F126, E127 and V128 form type IV helix turns, and other residues are also exposed to solvent. YsxC is present in the core region of the large 50S subunit and interacts with the S2 and S10 proteins of the small subunit of ribosome. The interface area or buried surface area of 1554 $Å^2$ leads to a high probability of interaction between these proteins, as shown by the HADDOCK docking solution and energy

Table 3 List of active and passive interface residues used to define ambiguous interaction restraints (AIRs) for docking, as well as flexible segments

YsxC	Active residues	L10, R33, Q57, Y81, K88, S89, H119, D124
	Passive residues	S13, L25, V36, R53, T54, Q56, G59, K60, T63, G82, K85, R91, D120, Q123, E145
	Flexible segments	I8–K16, L30–K38, I46–L64, P79–K93, I112–I127
L17	Active residues	E34, K38, E45, T101, K105, E115, E120
	Passive residues	E28, R29, R41, R102, L104, G107, V117, I118, L121, V122
	Flexible segments	S27–I48, Y100–P108, G113–V122
S2	Active residues	E116, K119, F126, E127, K131
	Passive residues	K112, E118, M120, E122, V128, P130, K132, K138, E140
	Flexible segments	R110–E122, F126–D142
S10	Active residues	K57, R62, N91, G95
	Passive residues	Y49, T50, H56, M88, G89, S94, V96, D97, E99, I100
	Flexible segments	V48–Q64, A86–K101

Table 4 Statistical analysis of HADDOCK results for each complex after clustering the solutions

Protein–protein complex	YsxC–L17	YsxC–S2	YsxC–S10
Haddock analysis of best cluster			
RMSD (Å)[a]	0.77±0.32	0.98±0.58	1.87±1.09
RMSD min (Å)[b]	1.54±0.09	5.48±0.24	4.66±0.62
CNS intermolecular energy after water refinement			
Haddock score			
E_{vdW} (kcal mol^{-1})[c]	−51.28±7.75	−34.71±3.59	−50.32±11.38
E_{ele} (kcal mol^{-1})[c]	−695.62±50.14	−403.48±127.81	−464.63±116.36
Buried surface area (Å^2)	2134±112	1416±156	1881±161
HADDOCK analysis of the best protein−protein complex from each cluster			
Interacting residues	YsxC	YsxC	YsxC
	R33, S55, Q56, Q57, Y81, G82, A84, K85, K88, R91, R118, H119, D120, P121, D124	L10, V15, R53, S55, Q57, G59, K60, T61	S13, T54, S55, Q57 G59, K60, T61, Q62, T63, N68, Q72, F75, P79, Y83, K88
	L17	S2	S10
	E28, R29, E34, K38, E45, T101, R102, K105, Q106, G107, E115, E120, L121, V122	E116, K119, D123, F126, E127, V128, P130, K131	V48, Y49, T50, H56, K57, R62, M88, G89, N91, S94, G95, V96, D97
Ramachandran plot assessment			
Residues in favored region (%)	85.0	82.8	85.8
Residues in additionally allowed region (%)	13.3	15.7	13.9
Residues in generously allowed region (%)	0.70	1.0	0
Residues in disallowed region (%)	1.0	0.5	0.4

Clusters are sorted according to average intermolecular energy

[a] Average RMSD and standard deviation of the lowest-energy structure of the cluster

[b] Average RMSD and standard deviation of the lowest-energy structure among all calculated structures

[c] The nonbonded energies were calculated with the OPLS parameters using an 8.5 Å cut-off

scores. The quality of the protein–protein bimolecular complex was assessed using a Ramachandran plot, which indicated high quality assurance, with >98% of the residues included in the allowed region (Table 4).

YsxC–S10 interactions

The N-terminal residues S13 and K85 of YsxC show stable H-bonding interactions with H56, G95, V96 and D97 of S10. These residues are also conserved in both the template and model structures. In addition, the part of the G2 motif that overlaps with the switch II region (T54, S55, Q57 G59, K60, T61, Q62, T63, N68, Q72, F75, P79, Y83 and K88) of YsxC also forms H-bonding and van der Waal interactions with the residues V48, Y49, T50, K57, R62, M88, G89, N91 and S94 in the S10 protein. Interacting residues of YsxC are mainly present in the N-terminal region and in part of the switch II region. In the case of the S10 protein, N91, S94 and V96 actively participate in a type IV β-turn, whereas H56 and Q57 are present in γ-turns. The residues V48, Y49 and T50 of S10 form a β-hairpin that is involved in hydrophobic interactions. The predicted intermolecular energy of the complex is −632 kcal mol^{-1}, which shows the stability of the bimolecular protein complex, and the YsxC–S10 protein complex is displayed in Fig. 10c. The S10 protein of the small subunit interacts with YsxC and is present at the core of the 50S subunit, which plays an important role in ribosome assembly. The high interface area (1980 Å^2) of this complex also supports the strength of the interaction. The Ramachandran plot indicates the quality of the protein–protein complex, with only 0.4% residues present in the disallowed region (Table 4).

Thus, the study of the interactions of YsxC with L17, S2 and S10 provides insight into the molecular interactions and importance of YsxC in ribosome assembly and stability. There is no such structural-level evidence for these protein

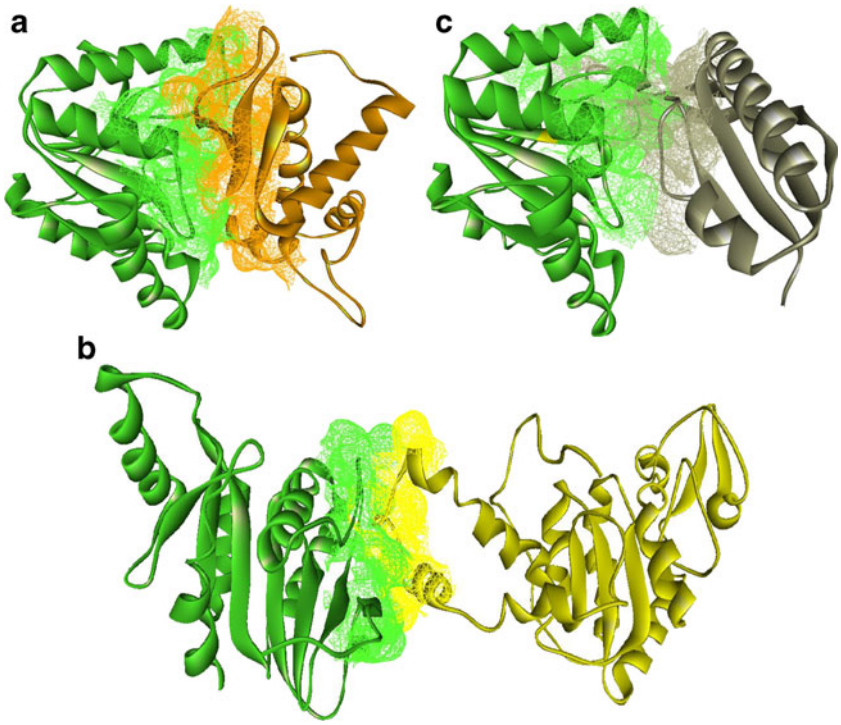

Fig. 10 **a**–**c** HADDOCK models of protein–protein complexes. **a** YsxC–L17, **b** YsxC–S2, **c** YsxC–S10. YsxC is presented in *green*; L17 in *orange*; S2 in *yellow*, and S10 in *gray*. The proteins are displayed as *cartoon sketches* and the interaction surface is shown as a *cloud*. The figures were prepared using Discovery Studio 2.0

complexes, so the results of this study support the experimental identification of the interactions of YsxC with L17, S2 and S10 at the structural level.

Alanine scanning mutagenesis

The interface residues of YsxC that are involved in interactions with the proteins L17, S2 and S10 were identified and used for further mutagenesis studies. The interface residues S55, Q57, G59, K60, T61 and K88 were mutated to alanine and structural mutants were generated. HADDOCK docking solutions for these YsxC mutants with other ribosomal binding proteins showed only minor interactions at the interfacial surface. The interaction score, based on the intermolecular energy and the RMSD deviation from the lowest-energy structure in the cluster, showed that the docked protein–protein complex is less stable. The intermolecular energies of the mutant YsxC–L17, YsxC–S2 and YsxC–S10 bimolecular complexes were found to be −318 kcal mol^{-1}, −184 kcal mol^{-1}, and −226 kcal mol^{-1}, respectively, which are much higher than those of the native complexes (data not shown here). These data indicate that the residues S55, Q57, G59, K60, T61 and K88 of YsxC interact strongly with the other ribosomal interacting proteins, as described for the protein–protein interaction analysis.

Stability analysis of the native protein complex

Docking analysis of the native YsxC with its ribosomal interaction partners shows energetically stable conformations of the bimolecular complexes, as confirmed by the molecular dynamics based trajectory analysis. The predicted hotspot residues of these protein complexes were shown to be stable throughout the 1 ns MD simulation. Conformational changes in the complexes during the simulation were gauged by monitoring the C_α RMSDs of each complex with respect to its starting structure. The RMSD values for the simulations are plotted in Fig. 11. As illustrated in the figure, the RMSDs for the protein complexes did not change after attaining their respective equilibria. The RMSD values for the YsxC–L17, YsxC–S2 and YsxC–S10 complexes were 0.3, 0.35, and 0.25 nm, respectively, after an average equilibrium period of 400 ps. The potential energies of the complexes were very low: -1.07×10^6, -2.82×10^6 and -8.85×10^5 kJ mol^{-1} for YsxC–L17, YsxC–S2 and YsxC–S10, respectively, which shows the stabilities of these complexes. Considering the results of this analysis, interactions of YsxC with L17, S2 and S10 are considered to be stable, which indicates that this protein–protein complex actively participates in ribosome assembly.

Proposed mechanism of YsxC interaction during ribosome assembly

MD simulation analysis and protein–protein interaction studies provide insight into the YsxC interaction mechanism during ribosome assembly. The average RMSF plot shows flexible motifs, loops and conserved core regions in the model structures, which may facilitate protein–protein

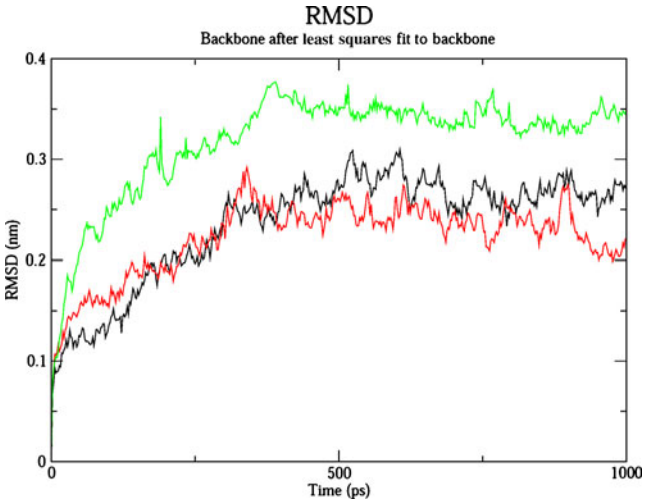

Fig. 11 MDS trajectory based analysis of protein–protein complexes: YsxC–L17, YsxC–S2 and YsxC–S10. The RMSDs of the Cα atoms with respect to the initial structures of the complexes show the stability of the model after the initial equilibration time. Color coding: *black* YsxC-L17, *green* YsxC-S2, *red* YsxC-S10

interactions or ligand binding (as discussed in the previous section). The substrate-binding sites and interface residues for protein–protein docking studies have been discussed in detail previously. RMSF analysis of the YsxC–GTP complex shows that substrate binding provides more flexibility at the interface site; i.e., the RMSF values for the residues S55–Q57, Y81–R91 and R118–D124 are ~0.64 nm, which is much higher than those of the other residues. The residues E28–K38, E45, T101–G107 and E115–V122 of the L17 protein, which have RMSF values of ~0.55 nm, interact with the YsxC protein to give the energetically stable heterodimer YsxC–L17 protein complex. In the presence of a ligand at the allosteric site, the interface residues of the active site show lower RMSF values, which indicate that these residues are not exposed to the solvent. This may be the reason for the reduced GTP-binding activity at the active site. Thus, allosteric inhibition is believed to inhibit ribosome assembly.

Similarly, the small proteins S2 and S10 of the 30S subunit approach the protein complex and form a hetero-tetramer (Fig. 12). RMSF analysis of the YsxC–L17 complex reveals that residues L10–V15 and R53–T61 of

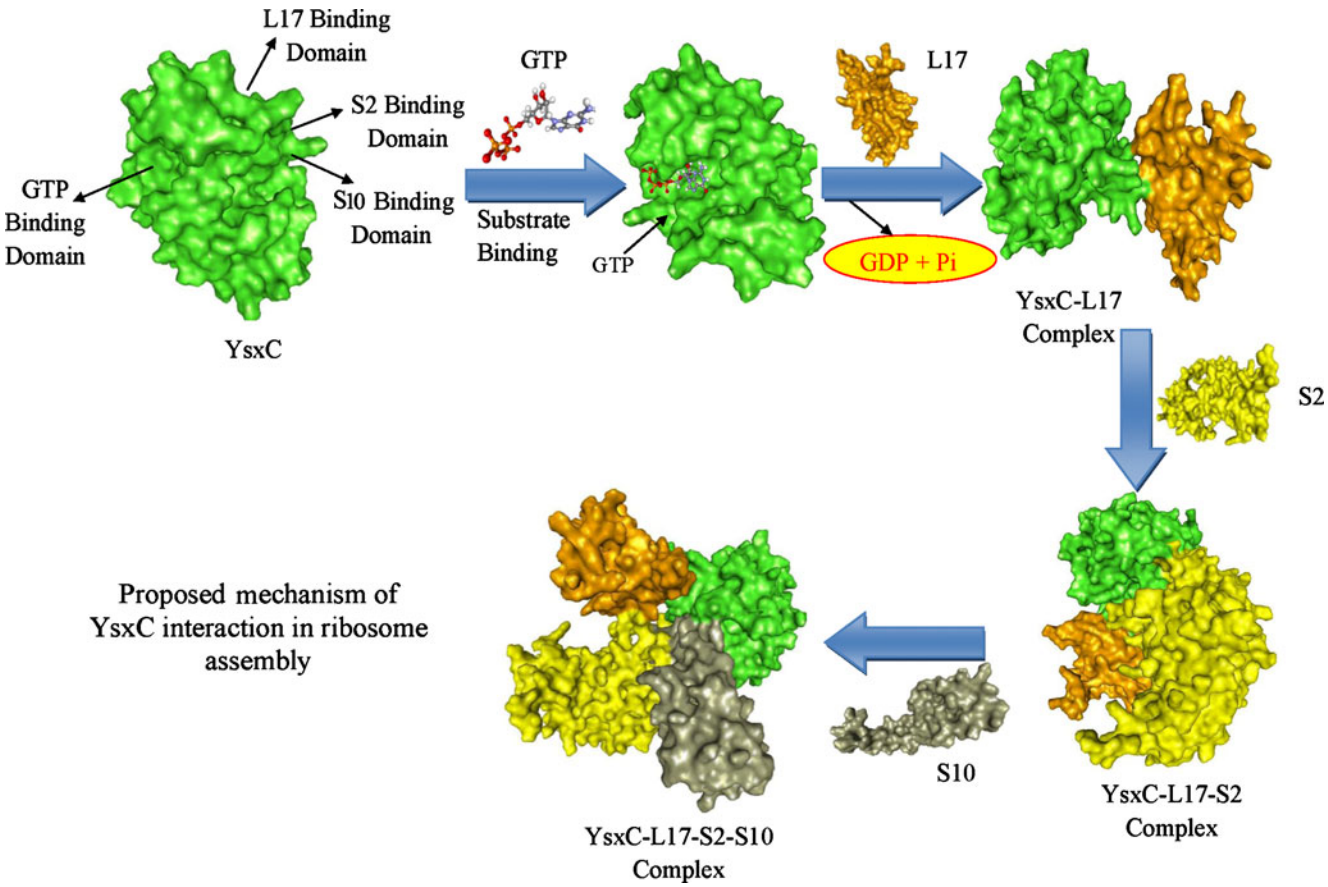

Fig. 12 Proposed mechanism of interaction of YsxC with its ribosomal interaction partners L17, S2, and S10. The GTP-binding, L17-binding, S2-binding and S10-binding domains are shown in the starting YsxC structure, and various complexes produced upon binding with GTP and various proteins are depicted. Color coding: *green* YsxC, *orange* L17, *yellow* S2, *gray* S10

YsxC have high RMSF values, more than 0.78 nm in this case, indicating a highly flexible region. These residues are involved in the interaction with the S2 protein, where residues E116–K119 and D123–K131 have RMSF values of around 0.58 nm, and these residues are similar to those predicted to occur at protein–protein interface sites. Furthermore, MD analysis of the YsxC–S2 complex shows that the residues T54–T63, N68–Q72 and P79–K88 of YsxC are highly flexible, with RMSF values of more than 0.70 nm. The abovementioned residues play significant roles in the interaction with the S10 protein, as confirmed by protein–protein docking studies. The change in conformation due to semi-flexible simulated annealing in an explicit 8 Å water layer, explored using the HADDOCK software, provides an exposed interface site that enhances the stability of the docked complex and also provides the solvent environment. However, the lower deviations seen in the RMSD profile of the protein–protein complex in MDS studies support the stability of the complex. Thus, the proposed mechanism shows the importance of YsxC in ribosome assembly.

Conclusions

The molecular model for YsxC in *S. aureus* has been predicted, and the mechanism of its interaction with L17, S2 and S10 was analyzed. The key hotspot residues involved in this interaction were identified, and they were confirmed through alanine scanning mutagenesis. Molecular dynamics analysis of these interactions and observations of the atomistic fluctuations induced by the binding of its interaction partners and their stabilities throughout the 3 ns of simulation helped to elucidate the novel mechanism of interaction between these proteins. In addition, residues in a binding cavity located near the GTP-binding site were found to produce allosteric inhibition of the binding of GTP, which in turn was found to affect the interactions between YsxC and its partners. Six potential ligands that were retrieved from a ligand database were observed to interact strongly with residues at the abovementioned site, and this interaction produces structural changes in the orientations of the residues involved in the binding of GTP. Molecular dynamics studies also confirmed the stability of the interactions between the six ligands and YsxC and explored the structural transformations induced by the binding of these ligands to the residues at the GTP-binding site. This observation suggests that it may be possible to inhibit the function of YsxC by designing specific inhibitors which can bind at the site that is hypothesized to have an allosteric effect on the binding of GTP. Though the obtained results lack experimental evidence, they can act as a guide, and may help in investigations of the function of YsxC at the molecular level as well as the design of novel inhibitors to treat the infections caused by *S. aureus.*

Acknowledgments RK, Manivel and Kannan thank the University Grants Commission, Government of India (UGC) for funding this Major Research Project, and the Rajiv Gandhi National Fellowship for also providing funding assistance. Research at the Laboratory of the Centre for Excellence in Bioinformatics, Pondicherry University, India is funded by the Department of Information Technology (DIT) and the Department of Biotechnology (DBT), Government of India, New Delhi, India.

References

1. Chambers HF (2005) Community-associated MRSA-resistance and virulence converge. N Engl J Med 352:1485–1487. doi:10.1056/NEJMe058023
2. NABI Biopharmaceuticals (2007) Key facts about *S. aureus* infections (2007) NABI Biopharmaceuticals, Miami. http://www.nabi.com. Accessed 10 April 2007
3. Lowy FD (1998) *Staphylococcus aureus* infections. N Engl J Med 339:520–530. doi:10.1056/NEJM199808203390806
4. Lindsay JA, Holden MT (2006) Understanding the rise of the superbug: investigation of the evolution and genomic variation of *Staphylococcus aureus*. Func Integr Genomics 6:186–201. doi:10.1007/s10142-005-0019-7
5. Tejerina C, Reig A, Codina J, Safont J, Baena P, Mirabet V (1992) An epidemiological study of burn patients hospitalized in Valencia, Spain during 1989. Burns 18:15–18. doi:10.1016/0305-4179(92)90112-8
6. Centers for Disease Control and Prevention (2003) Community-associated MRSA: frequently asked questions. Centers for Disease Control and Prevention, Atlanta. http://www.cdc.gov/ncidod. Accessed Aug 2003
7. Centers for Disease Control and Prevention. Community-associated MRSA: fact sheet (2003) Centers for Disease Control and Prevention, Atlanta. http://www.cdc.gov/ncidod. Accessed Feb 2003
8. Shopsin B, Mathema B, Martinez J, Ha E, Campo ML, Fierman A, Krasinski K, Kornblum J, Alcabes P, Waddington M et al (2000) Prevalence of methicillin-resistant and methicillin-susceptible *Staphylococcus aureus* in the community. J Infect Dis 182:359–362. doi:10.1086/315695
9. Keiichi H (2001) Vancomycin-resistant *Staphylococcus aureus*: a new model of antibiotic resistance. Lancet Infect Dis 1:147–155. doi:10.1016/S1473-3099(01)00091-3
10. Hutchison CA, Peterson SN, Gill SR, Cline RT, White O, Fraser CM, Smith HO, Venter JC (1999) Global transposon mutagenesis and a minimal Mycoplasma genome. Science 286:2165–2169. doi:10.1126/science.286.5447.2165
11. Schaefer L, Uicker WC, Wicker-Planquart C, Foucher AE, Jault JM, Britton RA (2006) Multiple GTPases participate in the assembly of the large ribosomal subunit in *Bacillus subtilis*. J Bacteriol 188:8252–8258. doi:10.1128/JB.01213-06
12. Cooper EL, García-Lara J, Foster SJ (2009) YsxC, an essential protein in *Staphylococcus aureus* crucial for ribosome assembly/stability. BMC Microbiol 9:266. doi:10.1186/1471-2180-9-266
13. Prágai Z, Harwood CR (2000) YsxC, a putative GTP-binding protein essential for growth of *Bacillus subtilis* 168. J Bacteriol 182:6819–6823
14. Wicker-Planquart C, Foucher AE, Louwagie M, Britton RA, Jault JM (2008) Interactions of an essential *Bacillus subtilis* GTPase,

YsxC, with ribosomes. J Bacteriol 190:681–690. doi:10.1128/JB.01193-07
15. Christopoulos A, May LT, Avlani VA, Sexton PM (2004) G-protein-coupled receptor allosterism: the promise and the problem (s). Biochem Soc Trans 32:873–877. doi:10.1042/BST0320873
16. May LT, Leach K, Sexton PM, Christopoulos A (2007) Allosteric modulation of G protein-coupled receptors. Annu Rev Pharmacol Toxicol 47:1–51. doi:10.1146/annurev.pharmtox.47.120505.105159
17. Ruzheinikov SN, Das SK, Sedelnikova SE, Baker PJ, Artymiuk PJ, Garcia-Lara J, Foster SJ, Rice DW (2004) Analysis of the open and closed conformations of the GTP-binding protein YsxC from *Bacillus subtilis*. J Mol Biol 339:265–278. doi:10.1016/j.jmb.2004.03.043
18. Vassylyev DG, Shirouzu M, Wada T, Yokoyama S (2009) The crystal structure of the bacteria-specific L17 ribosomal protein from *Thermus thermophilus*. doi:10.2210/pdb1gd8/pdb
19. Carter AP, Clemons WM, Brodersen DE, Morgan-Warren RJ, Wimberly BT, Ramakrishnan V (2000) Functional insights from the structure of the 30 S ribosomal subunit and its interactions with antibiotics. Nature 407:340–348. doi:10.1038/35030019
20. Gao H, Sengupta J, Valle M, Korostelev A, Eswar N, Stagg SM, van Roey P, Agrawal RK, Harvey ST, Sali A, Chapman MS, Frank J (2003) Study of the structural dynamics of the *E. coli* 70 S ribosome using real-space refinement. Cell 113:789–801. doi:10.1016/S0092-8674(03)00427-6
21. Larkin MA, Blackshields G, Brown NP, Chenna R, McGettigan PA, McWilliam H, Valentin F, Wallace IM, Wilm A, Lopez R, Thompson JD, Gibson TJ, Higgins DG (2007) Clustal W and Clustal X version 2.0. Bioinformatics 23:2947–2948. doi:10.1093/bioinformatics/btm404
22. Eswar N, Webb B, Marti-Renom MA, Madhusudhan M, Eramian D, Shen MY, Pieper U, Sali A (2007) Comparative protein structure modeling using MODELLER. Curr Protoc Protein Sci 50:2.9.1–2.9.31. doi:10.1002/0471140864.ps0209s50
23. Eramian D, Shen MY, Devos D, Melo F, Sali A, Marti-Renom MA (2006) A composite score for predicting errors in protein structure models. Protein Sci 15:1653–1666. doi:10.1110/ps.062095806
24. Hess B, Kutzner C, van der Spoel D, Lindahl E (2008) GROMACS 4: algorithms for highly efficient, load-balanced, and scalable molecular simulation. J Chem Theor Comput 4:435–447. doi:10.1021/ct700301q
25. Jorgensen WL, Maxwell DS, Tirado-Rives J (1996) Development and testing of the OPLS all-atom force field on conformational energetics and properties of organic liquids. J Am Chem Soc 118:11225–11236. doi:10.1021/ja9621760
26. Jorgensen WL, Chandrasekhar J, Madura JD, Impey RW, Klein ML (1983) Comparison of simple potential functions for simulating liquid water. J Chem Phys 79:926–935. doi:10.1063/1.445869
27. Kawata M, Nagashima U (2001) Particle mesh Ewald method for three-dimensional systems with two-dimensional periodicity. Chem Phys Lett 340:165–172. doi:10.1016/S0009-2614(01)00393-1
28. Hess B, Bekker H, Fraaije J, Berendsen HJC (1997) A linear constraint solver for molecular simulations. J Comput Chem 18:1463–1472. doi:10.1002/(SICI)1096-987X(199709)18:12<1463::AID-JCC4>3.0.CO;2-H
29. Miyamoto S, Kollman PA (1992) SETTLE—an analytical version of the shake and rattle algorithm for rigid water models. J Comput Chem 13:952–962. doi:10.1002/jcc.540130805
30. Martonák R, Laio A, Parrinello M (2003) Predicting crystal structures: the Parrinello–Rahman method revisited. Phys Rev Lett 90:075503. doi:10.1103/PhysRevLett.90.075503
31. Laskoswki RA, MacArthur MW, Moss DS, Thorton JM (1993) PROCHECK: a program to check the stereochemical quality of protein structures. J Appl Crystallogr 26:283–291. doi:10.1107/S0021889892009944
32. Colovos C, Yeates TO (1993) Verification of protein structures: patterns of nonbonded atomic interactions. Protein Sci 2:1511–1519. doi:10.1002/pro.5560020916
33. Luthy R, Bowie JU, Eisenberg D (1992) Assessment of protein models with three-dimensional profiles. Nature 356:83–85. doi:10.1038/356083a0
34. Brylinski M, Skolnick J (2008) A threading-based method (FINDSITE) for ligand binding site prediction and functional annotation. Proc Natl Acad Sci USA 105:129–134. doi:10.1073/pnas.0707684105
35. Laurie AT, Jackson RM (2005) Q-SiteFinder: an energy-based method for the prediction of protein–ligand binding sites. Bioinformatics 21:1908–1916. doi:10.1093/bioinformatics/bti315
36. Pagni M, Ioannidis V, Cerutti L, Zahn-Zabal M, Jongeneel CV, Hau J, Martin O, Kuznetsov D, Falquet L (2007) MyHits: improvements to an interactive resource for analyzing protein sequences. Nucleic Acids Res 35:W433–W437. doi:10.1093/nar/gkm352
37. Marchler-Bauer A, Anderson JB, Chitsaz F, Derbyshire MK, DeWeese-Scott C, Fong JH, Geer LY, Geer RC, Gonzales NR, Gwadz M, He S, Hurwitz DI, Jackson JD, Ke Z, Lanczycki CJ, Liebert CA, Liu C, Lu F, Lu S, Marchler GH, Mullokandov M, Song JS, Tasneem A, Thanki N, Yamashita RA, Zhang D, Zhang N, Bryant SH (2009) CDD: specific functional annotation with the Conserved Domain Database. Nucleic Acids Res 37(D):205–210. doi:10.1093/nar/gkn845
38. Marchler-Bauer A, Bryant SH (2004) CD-Search: protein domain annotations on the fly. Nucleic Acids Res 32(W):327–331. doi:10.1093/nar/gkh454
39. von Grotthuss M, Pas J, Rychlewski L (2003) Ligand-Info, searching for similar small compounds using index profiles. Bioinformatics 19:1041–1042. doi:10.1093/bioinformatics/btg117
40. Schuettelkopf AW, van Aalten DMF (2004) PRODRG—a tool for high-throughput crystallography of protein–ligand complexes. Acta Crystallogr D60:1355–1363. doi:10.1107/S0907444904011679
41. de Vries SJ, van Dijk ADJ, Bonvin AM (2006) WHISCY: what information does surface conservation yield? Application to data-driven docking. Protein Struct Funct Bioinf 63:479–489. doi:10.1002/prot.20842
42. Chen H, Zhou HX (2005) Prediction of interface residues in protein-protein complexes by a consensus neural network method: test against NMR data. Protein Struct Funct Bioinf 61:21–35. doi:10.1002/prot.20514
43. Zhou HX, Shan Y (2001) Prediction of protein interaction sites from sequence profiles and residue neighbor list. Protein Struct Funct Bioinf 44:336–343. doi:10.1002/prot.1099
44. Duhovny D, Nussinov R, Wolfson HJ (2002) Efficient unbound docking of rigid molecules. Lect Notes Comput Sci 2452:185–200. doi:10.1007/3-540-45784-4_14
45. Schneidman-Duhovny D, Inbar Y, Nussinov R, Wolfson HJ (2005) PatchDock and SymmDock: servers for rigid and symmetric docking. Nucleic Acids Res 33:W363–W367. doi:10.1093/nar/gki481
46. Andrusier N, Nussinov R, Wolfson HJ (2007) FireDock: fast interaction refinement in molecular docking. Protein Struct Funct Bioinf 69:139–159. doi:10.1002/prot.21495
47. Dominguez C, Boelens R, Bonvin AM (2003) HADDOCK: a protein–protein docking approach based on biochemical and/or biophysical information. J Am Chem Soc 125:1731–1737. doi:10.1021/ja026939x
48. de Vries SJ, van Dijk AD, Krzeminski M, van Dijk M, Thureau A, Hsu V, Wassenaar T, Bonvin AM (2007) HADDOCK versus HADDOCK: new features and performance of HADDOCK2.0 on

the CAPRI targets. Protein Struct Funct Bioinf 69:726–733. doi:10.1002/prot.21723
49. Wallace AC, Laskowski RA, Thornton JM (1995) LIGPLOT: a program to generate schematic diagrams of protein–ligand interactions. Protein Eng 8:127–134. doi:10.1093/protein/8.2.127
50. Lefèvre F, Rémy MH, Masson JM (1997) Alanine-stretch scanning mutagenesis: a simple and efficient method to probe protein structure and function. Nucleic Acids Res 25:447–448. doi:10.1093/nar/25.2.447
51. Feyfant E, Sali A, Fiser A (2007) Modeling mutations in protein structures. Protein Sci 16:2030–2041. doi:10.1110/ps.072855507
52. Ditlev EB, William MCJ, Andrew PC, Brian TW, Ramakrishnan V (2002) Crystal structure of the 30 S ribosomal subunit from *Thermus thermophilus*: structure of the proteins and their interactions with 16 S RNA. J Mol Biol 316:725–768. doi:10.1006/jmbi.2001.5359